



HAL
open science

Superconductors with structural chirality

Ryota Nakajima, Flavia Pop, Narcis Avarvari

► **To cite this version:**

Ryota Nakajima, Flavia Pop, Narcis Avarvari. Superconductors with structural chirality. *Journal of Materials Chemistry C*, 2024, 12 (32), pp.12207-12217. 10.1039/D4TC01719F . hal-04797451

HAL Id: hal-04797451

<https://univ-angers.hal.science/hal-04797451v1>

Submitted on 22 Nov 2024

HAL is a multi-disciplinary open access archive for the deposit and dissemination of scientific research documents, whether they are published or not. The documents may come from teaching and research institutions in France or abroad, or from public or private research centers.

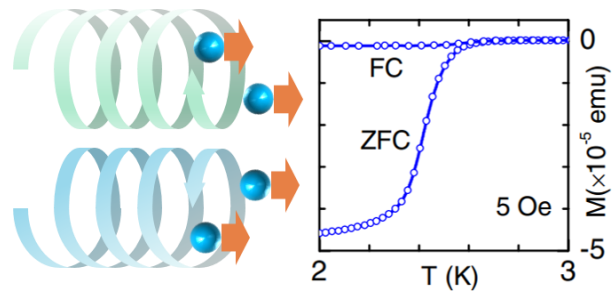
L'archive ouverte pluridisciplinaire **HAL**, est destinée au dépôt et à la diffusion de documents scientifiques de niveau recherche, publiés ou non, émanant des établissements d'enseignement et de recherche français ou étrangers, des laboratoires publics ou privés.

Superconductors with structural chirality

Ryota Nakajima,^{*a} Flavia Pop^a and Narcis Avarvari^{*a}

^a *Univ Angers, CNRS, MOLTECH-ANJOU, SFR MATRIX, F-49000 Angers, France. E-mail:*
ryota.nakajima@univ-angers.fr, narcis.avarvari@univ-angers.fr

Table of Content



We here discuss the development of inorganic and organic superconductors having a structural chirality.

Abstract

We discuss herein the so far reported chiral inorganic and organic superconductors with structural chirality. In chiral inorganic compounds, since the constituent atoms are not stable stereogenic centres, chirality can be reached by breaking improper rotation symmetry in a space group. These systems have anisotropic spin-orbit interaction and are therefore of interest from the viewpoint of the degree of freedom of the Cooper pairs and of the high upper critical magnetic field. We make here the distinction from chiral superconductivity that focuses on the topology of the Cooper pairs. Chiral superconductors derived from their non-centrosymmetric crystalline space groups, despite the achiral nature of the precursors, also exist in organic materials. The chirality induced spin selectivity (CISS) effect has been evidenced in an organic superconductor based on the bis(ethylenedithio)-tetrathiafulvalene (BEDT-TTF) donor. Although there have been reports of superconductivity in alkaline salts of polycyclic aromatic compounds, the existence of the phenomenon has been challenged. These issues are also discussed in this review. Furthermore, chirality can be addressed into organic materials by introducing stereogenic centres, which is a straightforward strategy to prepare chiral organic metals and, *a priori*, to achieve superconductivity. This review provides as well, besides a description of the structural chiral superconductors known to date, a summary of the main physical effects discovered in these materials, such as the electrical magnetochiral anisotropy (eMChA) and chirality induced spin selectivity (CISS) effects, and the main pieces of evidence reported in support for each of them.

1. Introduction

Chirality is one of the hottest topics in science attracting more and more researchers from different fields such as biology, physics, and chemistry. For example, in the latter, the asymmetric synthesis is one of the Holy Grails in organic chemistry since many years, particularly in the synthesis of pharmaceuticals, agrochemicals and natural products.^{1,2} Besides point stereogenic centres, consisting in atoms covalently linked to different substituents, there are also axial and planar chirality at the molecular level, plus the occurrence of chiral space groups in the solid state, where a chiral axis is expressed by the relative arrangement of two or more (a)chiral components. For these reasons, chirality was traditionally dominant through geometrical, biochemical and synthetic chemical aspects. In recent years, however, the physical aspects of chirality have also been studied extensively. Accordingly, the electrical magneto-chiral anisotropy (eMChA) effect is a typical chiral-dependent phenomenon translating the change in the magnetoresistance of a chiral (semi)conductor depending on the direction of the parallel/antiparallel magnetic field to the electric current.³ On the other hand, a spin-polarized electric current can be produced with a high polarization rate by passing an electric current through a chiral molecule. This is the so-called chirality induced spin selectivity (CISS) effect.⁴ Although the theory of the CISS effect has not yet been fully established, many theoretical and experimental studies have been attempted.⁵⁻⁸ They started with insulators due to simplicity at the material selection stage. The two effects, namely eMChA and CISS have been only recently reported in superconductors.^{9,10} In addition, much effort has been devoted over the years to the development of new superconducting materials and the elucidation of their theory, while the chiral superconductors remain comparatively limited in spite of their huge potential interest. This review is meant to bridge both chirality and superconductors fields. Note that chirality here refers to structural chirality, not to a distinction attributed to the topology of the Cooper pairs within the superconductor.¹¹

2. Chiral inorganic superconductors

Since the discovery of the superconductivity in Hg, many other superconducting materials have been explored.^{12,13} The high temperature systems, ferromagnetic systems, spin-triplet systems, and other unconventional systems have been studied in the inorganic chemistry research field.^{14,15} Non-centrosymmetric superconductors with broken inversion symmetry have also been developed and have attracted much attention in recent years.¹⁶

Eibenstein and Jung reported that isostructural $\text{Li}_2\text{Pd}_3\text{B}$ and $\text{Li}_2\text{Pt}_3\text{B}$ have antiperovskites-like structures, where six transition metal atoms are bonded to one boron in a distorted octahedral structure within Pd_6B or Pt_6B motifs (Fig. 1 for Pd_6B).¹⁷ Moreover, in $\text{Li}_2\text{Pd}_3\text{B}$ for example, one palladium atom has a coordination number of 14 (six palladium, two boron, six lithium) (Fig. 1). A palladium atom is also the vertex of another octahedron, forming a three-dimensional network.

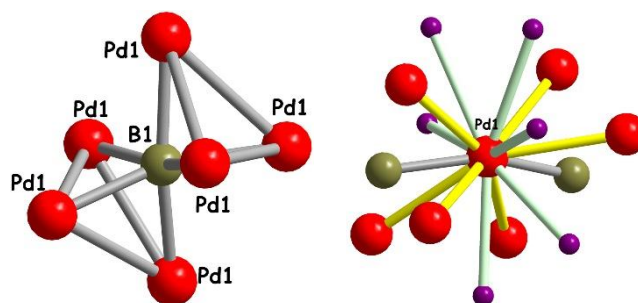


Fig. 1 Single crystal X-ray structure of $\text{Li}_2\text{Pd}_3\text{B}$ with a focus on the Pd_6B motif (left) and on the coordination sphere of one Pd atom (right). Colour code: atoms Pd (red), B (kaki), Li (violet).

The most interesting structural feature of these compounds is the enantiomorphic pair of chiral space groups, *i.e.* $P4_332$ and $P4_132$, in which they crystallized, although it is not clear from the several reports whether conglomerate or single enantiomeric crystals have been obtained. Judging from the difference of the reliability factors, the space group of $\text{Li}_2\text{Pd}_3\text{B}$ was inferred to be $P4_332$, but the difference from $P4_132$ was not conclusive in the case of $\text{Li}_2\text{Pt}_3\text{B}$. It is clear though that there is *a priori* no control on the occurrence of one or the other space group, therefore to date there is no report mentioning the preparation and study of

physical properties of both enantiomeric crystals with either Pd or Pt. The magnetic susceptibilities of polycrystalline samples in zero field cooling (ZFC) measurements show that the superconducting transition temperatures T_c are 6.7 K for $\text{Li}_2\text{Pd}_3\text{B}$ (approx. 8 K from resistivity measurements) and 2.43 K for $\text{Li}_2\text{Pt}_3\text{B}$ (Fig. 2 for $\text{Li}_2\text{Pd}_3\text{B}$).^{18,19}

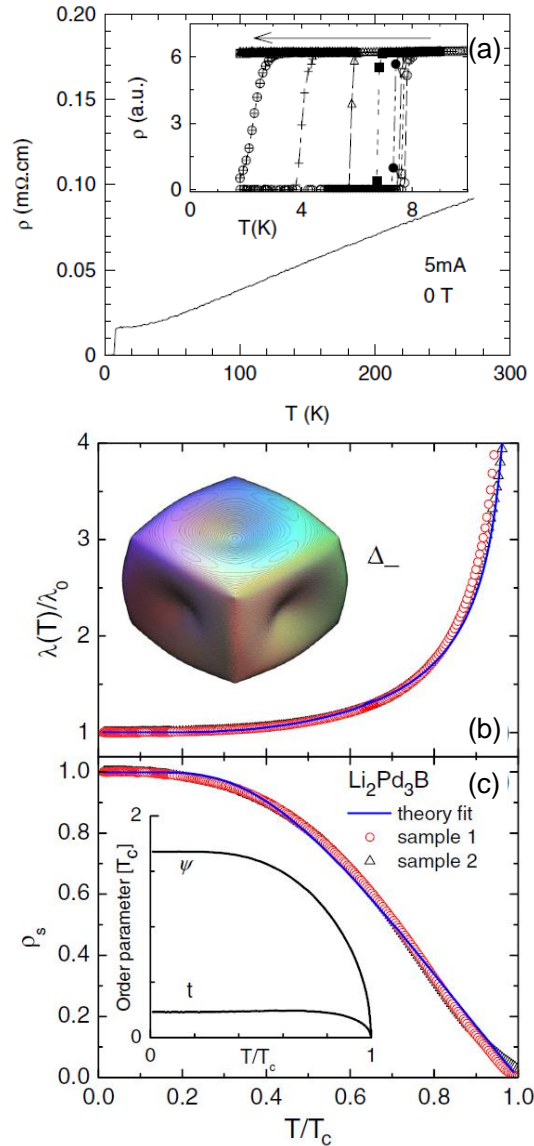


Fig. 2 Temperature-dependent resistivity measurements for crystalline $\text{Li}_2\text{Pd}_3\text{B}$. The inset shows the resistivity transition regions in applied magnetic fields H of 0, 0.05, 0.1, 0.2, 0.5, 1, 2, 3, 4, and 5 T (the arrow indicates the increase in H). The applied current was 5 mA for a 4-probe configuration (a). Reprinted with permission from ref. 18; Copyright 2004, The American Physical Society. The temperature dependence of (b) the normalized penetration depth $\lambda(T) / \lambda_0$ and (c) the corresponding superfluid density $\rho_s(T)$ for $\text{Li}_2\text{Pd}_3\text{B}$, in which $T_c = 7$ K, $G = 0.42$ nm/Hz for sample 1 and $T_c = 6.7$ K, $G = 0.63$ nm/Hz for sample 2. The symbols represent the experimental data and the solid line is a theoretical fit with parameters $\delta = 0.1$ and $\nu = 4$. The insets in the upper

panel and the lower panel show a 3D polar plot of the gap function $\Delta_{\mathbf{k}}$ and the temperature dependence of the order parameter components Ψ (spin singlet) and t (spin triplet), respectively (bottom). Reprinted with permission from ref. 19; Copyright 2006, The American Physical Society.

The BCS (Bardeen-Cooper-Schrieffer) theory, where the attractive force between two electrons has no directional dependence, can only allow the distribution of Cooper pairs to be isotropic.²⁰ In some non-BCS superconductors, the superconducting gap has nodes in certain regions of the Fermi surface. One of the methods to investigate the presence of nodes in the superconducting gap is to measure the temperature dependence of the superfluid density. The superconducting order parameters of these materials can be described by the magnetic field penetration length and the fitting calculation.²¹ The ratio of the spin-singlet order parameter Ψ and the spin-triplet order parameter t is defined as $\nu = \frac{\Psi}{t}$. The order parameter is calculated to be $\nu = 4$ for $\text{Li}_2\text{Pd}_3\text{B}$, which means that it is almost a spin-singlet state with cubed figure (Fig. 2). On the other hand, $\nu = 0.6$ for $\text{Li}_2\text{Pt}_3\text{B}$, indicating that the spin-triplet component is dominant. A broken inversion symmetry results in a mixed state of a spin-singlet and spin-triplet pairing, which produces an anisotropic superconducting order parameter. Interestingly, the critical temperature T_c is decreasing almost linearly with the amount of Pt (x) from 7.2 – 8 K for $\text{Li}_2\text{Pd}_3\text{B}$ to 2.2 – 2.8 K for $\text{Li}_2\text{Pt}_3\text{B}$ in the pseudo-binary solid solution $\text{Li}_2(\text{Pd}_{1-x}\text{Pt}_x)_3\text{B}$, $x = 0 - 1$.²²

TaRh_2B_2 and NbRh_2B_2 are superconductors with a chiral crystal structure reported by Carnicom, Cava *et al.*²³ Both compounds crystallized in the trigonal enantiomorphic space group $P3_1$, while its mirror-image counterpart $P3_2$ has not been observed. The Ta/Nb atoms form isolated spirals that are surrounded by boron-boron dimers. These spirals go through layers of Rh atoms arranged in a honeycomb lattice, with successive layers slightly shifted from the layer above and below, thus resulting in a spiral of Rh layers along the c axis (Fig. 3).

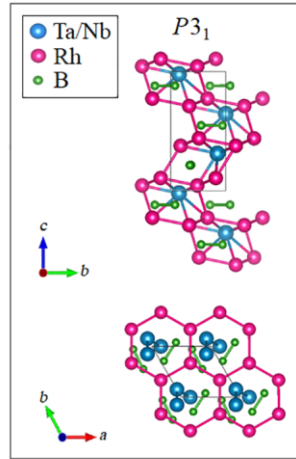


Fig. 3 Single crystal X-ray structure of Ta/NbRh₂B₂. Reprinted with permission from ref. 23; Copyright 2018, American Association for the Advancement of Science (AAAS).

The magnetic susceptibility in the ZFC process clearly exhibits a superconducting transition, with superconducting transition temperatures of 5.8 K for TaRh₂B₂ and 7.6 K for NbRh₂B₂. The electric resistivity measurements on compressed pellets indicate the same superconducting transition temperatures for the two materials (Fig. 4 for TaRh₂B₂).

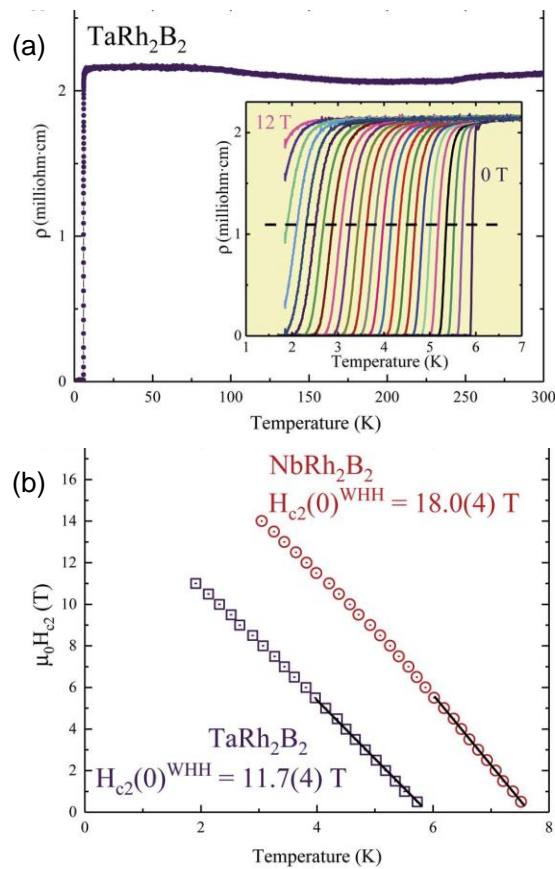


Fig. 4 Temperature-dependent electrical resistivity for TaRh₂B₂ (compressed pellet) measured from 300 to 1.7 K with no magnetic field. Inset: plot of the dependence of the superconducting transition on applied magnetic field

measured from 1.7 to 7 K in applied fields from 0 to 12 T. The dashed black line shows 50% of the superconducting transition (a). The T_c values at different applied fields were used to calculate the $\mu_0 H_{c2}(0)$ values for TaRh₂B₂ (11.7(4) T) and for NbRh₂B₂ (18.0(4) T) (b). Reprinted with permission from ref. 23; Copyright 2018, American Association for the Advancement of Science (AAAS).

The materials also exhibit progressive suppression of superconductivity under an applied magnetic field. TaRh₂B₂ still shows clear superconducting transition, accompanying a decrease in the transition temperature, even at 11 T applied field, while NbRh₂B₂ remains superconductor up to 14 T (Fig. 4). The upper critical field (H_{c2}) can be estimated following the Werthamer-Helfand-Hohenberg equation from the orbital pairing-breaking effect:

$$\mu_0 H_{c2}(0) = -0.693 T_c \frac{d\mu_0 H_{c2}}{dT}$$

where T_c denotes the critical temperature, $\frac{d\mu_0 H_{c2}}{dT}$ denotes the slope of $\mu_0 H_{c2}$ around T_c . By assigning $T_c = 5.8$ K for TaRh₂B₂ and $T_c = 7.6$ K, $\mu_0 H_{c2}(0)$ can be calculated to be 11.7 T and 18.0 T, respectively. On the other hand, the Pauli limit, where superconductivity is destroyed by the Zeeman effect, can be estimated as:

$$\mu_0 H^{Pauli} = 1.85 T_c$$

where T_c denotes the critical temperature. Thus, $\mu_0 H^{Pauli} = 10.7$ T for TaRh₂B₂ and $\mu_0 H^{Pauli} = 14.1$ T for NbRh₂B₂ are calculated. The existence of superconductivity beyond the Pauli limit means that the singlet Cooper pair is very likely broken and the superconducting state coexists with spins having degrees of freedom with some becoming triplets. This robustness against the applied magnetic fields is suggested to be due to the potential anomaly of chiral superconductors. This effect was also observed in the achiral non-centrosymmetric superconductor CePt₃Si¹⁶ and the achiral layered superconductor NbSe₂.²⁴

The solid solution system (Pt_{0.2}Ir_{0.8})₃Zr₅ is an achiral compound crystallizing in the centrosymmetric space group $P6_3/mcm$ at room temperature.²⁵ Interestingly, its purely bimetallic congeners Pt₃Zr₅ and Ir₃Zr₅ crystallize, at room temperature, in the non-chiral space

group $P6_3/mcm$ and in the enantiomorphic space group $P6_122$, respectively (Fig. 5).

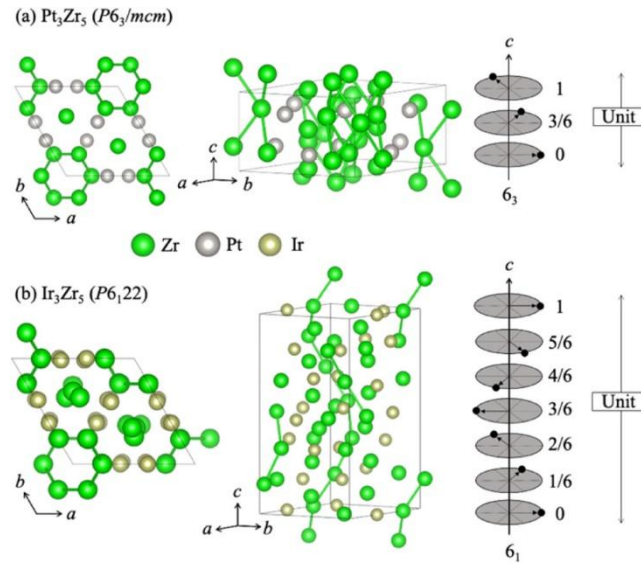


Fig. 5 Crystal structures of (a) Pt_3Zr_5 and (b) Ir_3Zr_5 . The figures on the left show the a - b plane views. In the middle are shown the structures along the c -axis. The figures on the right are the 6-fold screw axis 6_3 for Pt_3Zr_5 and 6_1 for Ir_3Zr_5 . Reprinted with permission from ref. 25; Copyright 2024, American Chemical Society.

Moreover, the former shows a superconducting transition at 6-7 K, while no superconductivity has been observed for the latter. Thus, the authors endeavoured to investigate the solid solutions $(Pt_{1-x}Ir_x)_3Zr_5$ for different nominal values of x , which showed that for $x = 0 \sim 0.85$ only the $P6_3/mcm$ phase was present at room temperature, whereas for $x = 0.9$ both $P6_3/mcm$ and $P6_122$ phases coexist. Finally, the phase $(Pt_{0.2}Ir_{0.8})_3Zr_5$ ($x = 0.8$) shows a temperature dependent structural phase transition from $P6_3/mcm$ to $P6_122$ upon cooling, such as the chiral space group $P6_122$ becomes dominant at low temperatures, accounting for 60% at 30 K. Magnetic susceptibility measurements showed a superconducting transitions for $x = 0 \sim 0.85$, with the T_c decreasing as x increases. Thus, for $(Pt_{0.2}Ir_{0.8})_3Zr_5$ it was estimated that chirality and superconductivity coexist. The existence of superconductivity was further confirmed by the temperature dependence of the specific heat. Electrical resistivity measurements also showed the onset of a superconducting transition temperature at 2.1 K for $(Pt_{0.2}Ir_{0.8})_3Zr_5$, with the superconducting state resisting up to a magnetic field of 0.1 T (Fig. 6).

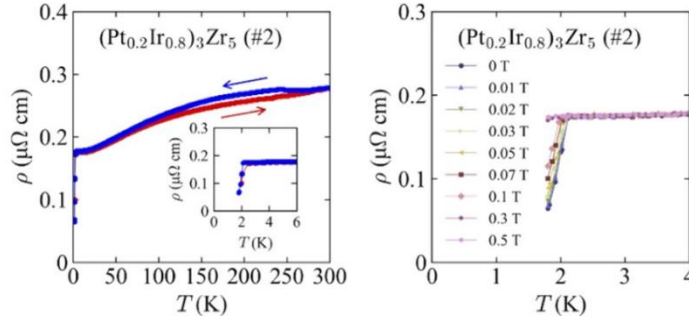


Fig. 6 Temperature dependence of ρ in the cooling and heating processes for $(\text{Pt}_{0.2}\text{Ir}_{0.8})_3\text{Zr}_5$. The inset is the enlarged view at $T \leq 6 \text{ K}$ (left). $\rho(T)$ under several applied magnetic fields for $(\text{Pt}_{0.2}\text{Ir}_{0.8})_3\text{Zr}_5$ (right). Reprinted with permission from ref. 25; Copyright 2024, American Chemical Society.

However, the estimated upper critical field is 2.59 T, whereas the Pauli limit $\mu_0 H^{Pauli}$ reaches 4.08 T. Since the critical field calculated by the Werthamer-Helfand-Hohenberg equation is 1.33 T, the mechanism of the upper critical field of this material is dominated by the orbital pairing-breaking effect. Therefore, the anisotropy spin orbit coupling effect, often seen in chiral superconductors, does not contribute significantly here to the physical properties of this material. It should be pointed out that in the composition of $(\text{Pt}_{0.2}\text{Ir}_{0.8})_3\text{Zr}_5$ only transition metals are present, therefore orbital hybridization is not likely to occur, which should not provide a significant antisymmetric spin-orbit coupling (ASOC). On the contrary, the chiral superconductors TaRh_2B_2 and NbRh_2B_2 discussed above contain transition metals and boron, which could explain the observed Pauli limit violation thanks to the orbital hybridization between p and d orbitals. Thus, the crystal structure and elemental composition can be important parameters for the ASOC.

Carbon nanotubes (CNT) are remarkable materials possessing unique electronic, thermal, and optical properties as well as high physical strength and chemical reactivity.²⁶ Many related applications have been considered in various research fields,²⁷ and even signature of superconductivity has been claimed.²⁸ Inorganic derivatives of CNT have been developed as well. As such, tungsten disulfide (WS_2) is a metal dichalcogenide semiconductor material, consisting in a three-layer S-W-S sandwich structure with covalent tetrahedral W-S bonds,

where faint van der Waals bonds connect adjacent sulfur sheets. It can be obtained as a variety of polyhedral and cylindrical forms including nanotubes,²⁹ that exhibit superconductivity with applied gate voltage.⁹ There are three structural types of WS₂ nanotubes: zig-zag, armchair type and chiral type. These can be distinguished by TEM diffraction patterns. F. Qin *et al.* assembled the device with ionic liquid gating. WS₂ nanotubes where zig-zag type domains and chiral type domains coexist were placed on the electrodes, and KClO₄/polyethylene glycol electrolyte as the gate medium is bridged upon the gate terminal and the sample. With an ionic liquid gate, the same sign ions build up, forming an electric double layer on the semiconductor surface, and high density carriers are accumulated. In addition, voltage can be applied until an electrochemical reaction occurs in the electric double layer, so that high electric fields and high carrier densities can be achieved with low voltages.³⁰ The WS₂ nanotube undergoes the superconducting transition under 8 V gate voltage at 5.8 K. The chiral signature is expressed as a non-reciprocal electron transport in the superconducting regime, in which the forward and backward supercurrent flows are not equivalent because of inversion symmetry breaking, as a consequence of the electrical magnetochiral anisotropy (eMChA) effect (Fig. 7).

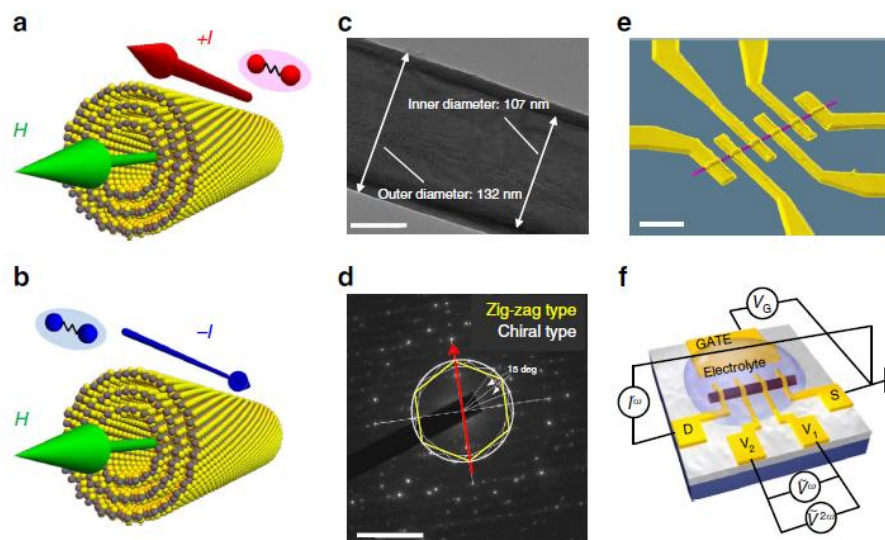


Fig. 7 WS₂ chiral NT and asymmetric superconducting transport in chiral NTs. (a,b) Illustrations of the unidirectional electric transport in superconducting chiral NT. Because of the broken inversion symmetry, asymmetric magnetoresistance is expected under magnetic field parallel to the tube axis. (c) Transmission

electron microscopy (TEM) image of a single WS₂ NT. (d) Electron diffraction pattern of a single WS₂ NT. The red arrow represents the direction of the tube axis. Tilted hexagonal diffraction pattern (white lines) confirms the chiral structure in addition to the zigzag type NT (yellow line). (e) SEM image of a WS₂ NT device. (f) Illustration of the electric double-layer transistor device. The electrolyte KClO₄/polyethylene glycol is used as gate medium. Reproduced with permission from ref. 29. Copyright 2017 Nature Publishing Group.

Based on symmetry arguments, the electrical resistance under a parallel magnetic field can be expressed as:

$$R(I, H) = R(-I, -H) = R_0(1 + \gamma I \mu_0 H)$$

where γ denotes a gyrotropic coefficient, I denotes an electric current, μ_0 denotes a magnetic constant, H denotes a magnetic field.

By applying an alternating current (AC), this second term can be expressed in voltage as:

$$V^{2\omega}(t) = \frac{1}{2} \gamma R_0 \mu_0 H I_0^2 \left\{ 1 + \sin \left(2\omega t - \frac{\pi}{2} \right) \right\}$$

In the lock-in measurement, the resistance of the eMChA effect can be expressed as follows by taking the term at $2\omega t$ shifted by $\frac{\pi}{2}$.

$$R^{2\omega} = \frac{1}{2} \gamma R_0 \mu_0 H I$$

$R^{2\omega}$ gives an antisymmetric signal with the applied magnetic field at low temperatures. The magnitude of the magnetic resistance varies depending on the relative angle between the electric current and the magnetic field. Thus, the eMChA effect was demonstrated for the first time in a chiral superconductor.

Worth noting, although not involving structurally chiral superconductors but heterostructures, is the observation of unconventional order parameter probed by low-temperature scanning tunnelling microscopy and of unconventional Meissner response induced by the adsorption of chiral molecules on the surface of classical superconductors such as Nb and NbSe₂,^{31–33} or in

chiral hybrid TaS₂ superlattices obtained by the intercalation of chiral molecules.³⁴ This endeavour enables the possibility of CISS experiments in superconducting materials to considerably expand. In addition to that, two-dimensional diatomic honeycomb lattices are theoretically predicted to produce chiral phonons.³⁵

3. Chiral organic superconductors

3.1 Superconductivity issues in alkali salts of polycyclic aromatic hydrocarbons

Superconductivity within alkali-doped polycyclic aromatic hydrocarbons (PAHs), in which the π -electron system is widely delocalized on their conjugated framework, has been claimed first in 2010 in potassium-doped picene K_xpicene ($x = 2.9$ or 3.3), with a reported $T_c = 18$ K.³⁶ These materials, together with the alkali-doped phenanthrene materials, i.e. A₃phenanthrene ($A = \text{K}$ or Rb), $T_c \approx 5$ K,³⁷ and K-doped dibenzopentacene, K_xdibenzopentacene, $T_c = 33$ K, produced a massive burst of interest in the community.³⁸ Although the PAH involved in these materials are not chiral themselves, it is worth mentioning these results in the context of this review with respect to the possibility to generate such reduced species with inherently chiral helicenes, which are helical PAHs.³⁹⁻⁴¹ Moreover, picene and phenanthrene molecules are zig-zag shaped aromatic hydrocarbons and form two-dimensionally herringbone structures in the a - b plane, which crystallize in the chiral space group $P2_1$, making their conducting doped derivatives virtually chiral from the structural point of view. The general composition formula of these “salts” is thus A_x(PAH), where A denotes K or Rb. The alkali metal is intercalated into the crystal voids, keeping *a priori* the same packing between the neutral and the doped PAH. Different annealing temperature, time and constituent ratio conditions can produce various types of samples. The highest transition temperature was recorded at 18 K with K_{3.3}Picene, where the ZFC magnetic measurement shows a drastic decrease of the magnetic susceptibility. However, these studies have been questioned and doubted in terms of molecular instability of the PAH alkaline salts and impurities in the samples. The attempts to

reproduce these experiments by Heguri, Kobayashi and Tanigaki indicate the thermodynamic instability of the phenanthrene doped phase and decomposition of the PAH in the reaction conditions.⁴² After annealing for twenty hours, indeed X-ray diffraction (XRD) profiles exhibit broad peaks corresponding to the metal hydride, implying the PAHs are decomposed by hydrogen breakaway. The samples contain small amounts of ferromagnetic fragments that produced the residual magnetization. No proofs corresponding to superconductivity were observed for K_x phenanthrene ($x = 1-3$) above 2 K, therefore the occurrence of superconducting states in $A_x(\text{phenanthrene/picene})$ ($A = K$ or Rb) seem extremely unlikely. Additional proofs in this respect have been provided by Rosseinsky and Prassides who succeeded to prepare in pure crystalline form K_2 pentacene and K_2 picene by a solid state insertion protocol using potassium hydride as reducing agent,⁴³ and also $CsC_{14}H_{10}$ and $Cs_2C_{14}H_{10}$ ($C_{14}H_{10} = \text{phenanthrene}$), obtained by reduction of phenanthrene with metallic caesium in anhydrous THF.⁴⁴ Neither of these salts showed, unfortunately, superconducting behavior above 2 K.

3.2 Organic chiral superconductors

The development of superconductors in organic materials has mainly started with the tetrathiafulvalene (TTF) derivatives.⁴⁵ Indeed, the selenium substitute tetramethyl-tetraselenafulvalene (TMTSF) based conductor $(TMTSF)_2PF_6$ is the first example of organic superconductors, with $T_c = 0.9$ under 12 kbar.^{46,47} Triggered by this milestone discovery, a large number of TTF based superconductors have been developed for the last several decades.⁴⁸⁻⁵¹ Particularly interesting is the κ -(BEDT-TTF) $_2$ ·Cu(NCS) $_2$ material synthesized by Mori, Saito *et al.*, exhibiting ambient pressure superconductivity, with a T_c of 10.4 K, as well as chirality, despite the achiral nature of its organic and inorganic components.⁵² Accordingly, the crystalline salt is composed of dimeric mixed valence radical cations of bis(ethylenedithio)-TTF (BEDT-TTF), namely $[(BEDT-TTF)_2]^+$, and of counterions

$[\text{Cu}(\text{NCS})_2]^-$, forming polymeric chains which impart chirality to the crystal. The BEDT-TTF dimers arrange almost perpendicularly to each other, resulting in a κ -type arrangement. The conducting pass is spread two dimensionally, separated by $[\text{Cu}(\text{NCS})_2]_n$ anionic chains. As already mentioned, both constituents are achiral, but the winding polymeric inorganic chains, which are non-centrosymmetric, imprint a chiral structure at the crystal level, resulting in the non-centrosymmetric space group $P2_1$, with the 2_1 screw axis running along the b -axis. According to electron diffraction experiments of thin crystals, the d -form crystals are often obtained.⁵³ The electrical resistivity measurement show metallic behaviour down to 250 K, which then turns into semiconducting behaviour down to 90 K. This upturn of the resistivity corresponds to a Mott transition, where the stabilization energy due to the localization of the electrons becomes dominant. After reaching the highest value, the resistivity decreases rapidly and vanishes around 10 K. The superconducting transition temperature defined as the middle of the transition is 10.4 K. Due to its strong two-dimensionality, this material is known to form a pancake-shaped vortex where the superconducting vortices are layered and split, each of them being linked by Josephson junctions.⁵⁴ Somehow surprisingly when considering its “birth” back to 1988, the research exploiting the chirality of this material has been engaged only very recently by Yamamoto *et al.*,¹⁰ certainly one of the related difficulties being the access to homochiral crystals. Here the authors obtained very thin crystals, by adapting the classical electrocrystallization technique, which were mapped by CD microscopy in order to characterize them chiroptically. While most of the crystals showed indeed the same chirality, in accordance with ref. 53, some crystals contained both opposite chiral domains as well. The critical temperature value of the superconducting transition of the thin crystals was $T_c = 7.4$ K, that is lower than the one reported for the bulk crystals. By applying AC current on a homochiral crystal, an antisymmetric field dependence appeared on the magnetic electrode (Fig. 8).

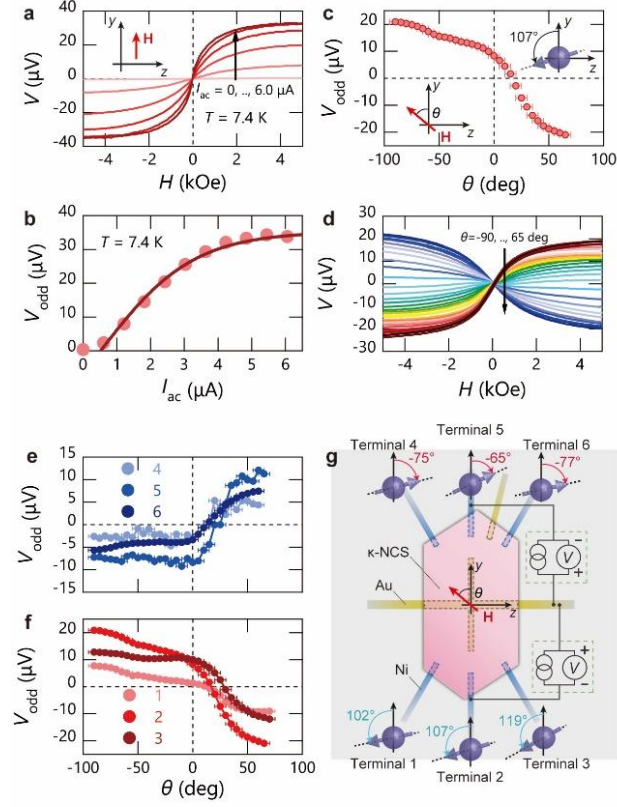


Fig. 8 (a) H dependence of voltage drop. $I_{a.c.}$ is the magnitude of an a.c. excitation applied to the device. The interval of $I_{a.c.}$ is $1.2 \mu\text{A}$. (b) $I_{a.c.}$ dependence of V_{odd} . The solid line is a guide to the eye. (c) Angular dependence of V_{odd} . θ is the angle of H measured from the y axis, shown in the inset at the lower left. The inset at the upper right shows the direction of the spins accumulated near the interface. $V_{a.c.}$ was set to 100 mV . (d) H dependence of V at different values of θ at intervals of 5° . (e,f) θ dependence of V_{odd} measured at the detection terminals along positive y (e) and negative y (f). $V_{a.c.}$ was set to 100 mV . (g) Spatial distribution of the spin accumulation, calculated from (e) and (f). Reproduced with permission from ref. 10. Copyright 2023 Nature Publishing Group.

Considering the fact that spin injection can be detected as voltage depending on the potential shift in a magnetic electrode, this voltage signal expresses the spin polarization *via* the CISS effect in the superconducting state. Normally, the spin polarization in a gyrotropic superconductor is generated by the Edelstein effect following the equation⁵⁵⁻⁵⁷:

$$\delta n = \mathbf{T} \tilde{\mathbf{J}}_e$$

where δn denotes the spin polarization density, \mathbf{T} denotes a component of the magnetoresistance tensor, and $\tilde{\mathbf{J}}_e$ denotes a supercurrent density. Accordingly, the Edelstein effect V_{Edel} is estimated as:

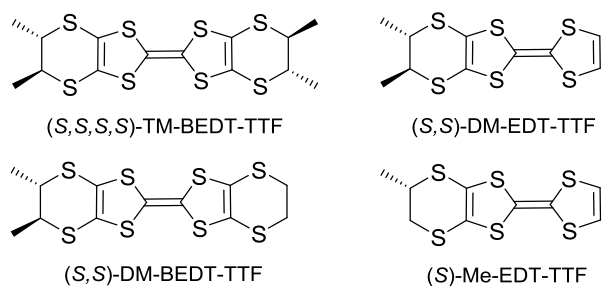
$$V_{Edel} \sim P^F \delta n_{int}^F / \{e N_{min}^F(E_F)\}$$

where P^F denotes the equilibrium spin polarization and $N_{min}^F(E_F)$ denotes the density of states for the minority spin at the Fermi level of nickel. In the case of κ -(BEDT-TTF)₂·Cu(NCS)₂ a voltage value $V_{Edel} < 26$ nV, corresponding the Edelstein effect, was calculated. When considering the experimental voltage value defined as $V_{odd} = [V(+5 \text{ kOe}) - V(-5 \text{ kOe})]/2$, which is in the μV range (Fig. 8), this means the spin-polarized current through the CISS effect was three orders of magnitude larger than the conventional theory. Not only giant spin polarization, but also determination of the spin direction by the CISS effect in the chiral superconductor was achieved, together with the observation of pairs of antiparallel spins. The typical concept of the CISS effect, which is the spin polarization of electrons tunnelling through chiral molecules, only involves T -even quantities. However, inward and outward switching of pairs of antiparallel polarized spins can be performed by both time-reversal (T) and mirror (m) operations, which are considered as T -odd chirality. Considering that the chirality of the material is T -even, this result proves that spins can reflect the lattice chirality of a chiral superconductor through the CISS effect, and indicates that the conversion from T -even chirality to T -odd chirality is feasible. Since the measurement temperature corresponds to the midpoint of the superconducting transition, superconducting vortices should be mixed in a metallic phase. No spin polarization is detected in a completely superconducting state. Thus, the spin carriers might also originate from Bogoliubov quasi-particles which are constructed by superpositions of excitations of negative charged electrons and positive charged electron holes. These outstanding manifestations of the CISS effect were realized by considering the superconductor as a single chiral molecule due to the macroscopic coherence length. Incorporating the concept of time-reversal symmetry into superconductors enables the study of new superconducting devices that make full use of chirality and superconductivity.

In the previous example the structural chirality occurred in a serendipitous manner thanks to

the polymeric zig-zag shape of the anion which is however achiral in its molecular form. The combination of chiral anions, provided with controlled chirality through stereogenic centres, with benchmark TTF donors, such as BEDT-TTF or 2,5-bis(1,3-dithiolan-2-ylidene)-1,3,4,6-tetrathiapentalene (BDH-TTP), is a promising strategy towards chiral organic superconductors, investigated especially by Martin *et al.*^{58,59} However, so far only chiral metallic compounds have been reported.

The alternative strategy consists in the combination of chiral TTF derivatives with achiral anions, thus opening many more possibilities of exploration than the previous one, since the number of chiral anions suitable to provide crystalline radical cation salts is relatively limited. As such, a consistent number of molecular conductors with chiral ethylenedithio-TTF (EDT-TTF) and BEDT-TTF derivatives,⁶⁰ especially containing methyl substituents on the ethylene bridges (Scheme 1), have been reported and their conducting properties investigated.⁶¹⁻⁶⁵ Note the first observation of the eMChA effect in a bulk crystalline chiral metal, namely (DM-EDT-TTF)₂ClO₄.⁶⁶



Scheme 1 Chiral TTF derivative candidates for chiral organic superconductors. Only the (*S*) enantiomers are shown.

However, the chiral conductors based on this strategy reported so far showed at best metallic conductivity. A special case, worth to discuss in the context of the present review, is the κ -[(*S,S*)-(DM-BEDT-TTF)]₂·ClO₄ compound reported in 1992 by Zambounis *et al.* as being superconductor below 2 K under applied moderate pressure of ≈ 5 kbar.⁶⁷ Since no further report confirming the claimed superconducting transition, combined with the fact that only the (*S*) enantiomer has been described, prompted us to re-investigate these chiral conductors in a

more consistent manner, by synthesizing both enantiomeric salts.⁶⁸ The donors in the crystal form strong face-to-face mixed-valence radical cations dimers which build up a κ -type arrangement. There are four independent donor molecules in the unit cell and, remarkably, they pair two by two in two different κ -layers (Layer 1 and Layer 2), a very original feature. According to the DFT band structure calculations, Layer 1 provides a 1D dispersion band, whereas Layer 2 forms a typical 2D band. The charge distribution on the donors indicate that the donors in Layer 1 are slightly more oxidized ($\approx +0.6$) than those in Layer 2 ($\approx +0.4$). Unlike the initial report claiming superconductivity in the (*S*) enantiomer under pressure, the new resistivity measurements performed on several crystals of each enantiomer revealed metallic behaviour in the high temperature regime and an upturn of the resistivity below 80 K at ambient pressure, as a consequence of a Mott insulating state. As pressure is applied, the room temperature electric resistivity decreases and the metal-insulator transition was pushed down to 10 K at 14.5 kbar, yet with no evidence of superconductivity. However, one of the measured samples showed an abrupt drop of resistivity to almost zero below 1 K under a pressure of 7.5 kbar upon increasing the current density. This resistivity drop was insensitive to applied magnetic field, which is contrary to the occurrence of a superconducting state. The behaviour observed here is very likely reminiscent of a current-induced melting of a charge ordered state and definitely not of a superconducting transition. Throughout these examples it appears that although no chiral superconductors based on chiral TTF derivatives have been obtained to date, the endeavour of several research groups will most probably afford such materials. Moreover, another promising family of conducting molecular materials which can provide superconductors are the metal bis(dithiolene) complexes,⁶⁹ although embedding chirality in such precursors is more recent compared to TTFs.^{70,71}

4. Summary and outlook

Several superconductors with structural chirality and their related physical properties have

been discussed in this review. It has been shown that various materials, both inorganic and organic, have superconducting phases (Table 1), and, sometimes, superconductivity has been achieved with some physical doping. The most critical issue is clearly the access to potential superconducting materials with controlled structural chirality. In the inorganic case the serendipitous crystallization in chiral space groups does not allow to choose one or another enantiomer. This is the case also with the so far unique chiral TTF based superconductor where symmetry breaking arises upon formation of the polymeric anionic chains during crystallization. Very likely, the most promising strategy in the case of organic superconductors is the use of precursors which are chiral themselves. A couple of examples of chiral materials for which the occurrence of superconductivity has been invalidated has been discussed as well, thus emphasizing an unwavering interest of the communities of chemistry and physics of chirality, molecular conductors and solid state physics. Researches into superconducting quantum computers and other more recent areas of superconductivity have been active in the last decade. Therefore, the use of chiral superconductors showing spin polarization and/or charge rectification could be effectively utilised to study superconducting spintronics incorporating spin interconnections. These cross-disciplinary researches greatly stimulate the investigations of chiral-dependent phenomena and contribute to the development of new functional materials.

Table 1 Summary of the reported critical temperatures for superconductors with structural chirality

Compounds	Transition temperatures (K)
$\text{Li}_2\text{Pd}_3\text{B}$	6.7
$\text{Li}_2\text{Pt}_3\text{B}$	2.43
TaRh_2B_2	5.8
NbRh_2B_2	7.6
$(\text{Pt}_{0.2}\text{Ir}_{0.8})_3\text{Zr}_5$	2.1
WS_2	5.8 (gate voltage: 8 V)
$\kappa\text{-(BEDT-TTF)}_2\cdot\text{Cu(NCS)}_2$	10.4

$K_{3,3}$ Picene	18 (impure materials)
$[(S,S)\text{-(DM-BEDT-TTF)}]_2\cdot\text{ClO}_4$	~ 1 (5.8 kbar) (invalidated)

Conflicts of interest

There are no conflicts to declare.

Acknowledgements

This work was supported by the CNRS through the Emergence Program (postdoctoral support to R.N.), the University of Angers and the French National Agency for Research (ANR) project SECRETS (ANR PRC 20-CE06-0023-01).

References

- [1] T. P. Yoon and E. N. Jacobsen, *Science*, 2003, **299**, 1691-1693
- [2] P. S. Steinlandt, L. Zhang and E. Meggers, *Chem. Rev.*, 2023, **123**, 4764-4794
- [3] G. L. J. A. Rikken, J. Fölling and P. Wyder, *Phys. Rev. Lett.*, 2001, **87**, 236602
- [4] K. Ray, S. P. Ananthavel, D. H. Waldeck and R. Naaman, *Science*, 1999, **283**, 814-816
- [5] J. Kishine, H. Kusunose and H. M. Yamamoto, *Isr. J. Chem.*, 2022, **62**, e202200049
- [6] G. L. J. A. Rikken and N. Avarvari, *J. Phys. Chem. Lett.*, 2023, **14**, 9727-9731
- [7] B. Göhler, V. Hamelbeck, T. Z. Markus, M. Kettner, G. F. Hanne, Z. Vager, R. Naaman and H. Zacharias, *Science*, 2011, **331**, 894-897
- [8] K. Banerjee-Ghosh, O. B. Dor, F. Tassinari, E. Capua, S. Yochelis, A. Capua, S-H. Yang, S. S. P. Parkin, S. Sarkar, L. Kronik, L. T. Baczewski, R. Naaman and Y. Paltiel, *Science*, 2018, **360**, 1331-1334
- [9] F. Qin, W. Shi, T. Ideue, M. Yoshida, A. Zak, R. Tenne, T. Kikitsu, D. Inoue, D. Hashizume and Y. Iwasa, *Nat. Commun.*, 2017, **8**, 14465
- [10] R. Nakajima, H. Daichi, G. Kawaguchi, Y. Nabei, S. Takuro, T. Narushima, H. Okamoto

- and H. M. Yamamoto, *Nature*, 2023, **613**, 479-484
- [11] W. Qin, L. Li and Z. Zhang, *Nat. Phys.*, 2019, **15**, 796-802
- [12] H. K. Onnes, *Commun. Phys. Lab. Univ. Leiden*, 1911, **12**, 120
- [13] C. Tresca, G. Profeta, G. Marini, G. B. Bachelet, A. Sanna, M. Calandra and L. Boeri, *Phys. Rev. B*, 2022, **106**, L180501
- [14] M. K. Wu, J. R. Ashburn, C. J. Torng, P. H. Hor, R. L. Meng, L. Gao, Z. J. Huang, Y. Q. Wang and C. W. Chu, *Phys. Rev. Lett.*, 1987, **58**, 908-910
- [15] S. S. Saxena, P. Agarwal, K. Ahilan, F. M. Grosche, R. K. W. Haselwimmer, M. J. Steiner, E. Pugh, I. R. Walker, S. R. Julian, P. Monthoux, G. G. Lonzarich, A. Huxley, I. Sheikin, D. Braithwaite and J. Flouquet, *Nature*, 2000, **406**, 587-592
- [16] E. Bauer, G. Hilscher, H. Michor, Ch. Paul, E. W. Scheidt, A. Griбанov, Yu. Seropegin, H. Noël, M. Sigrist and P. Rogl, *Phys. Rev. Lett.*, 2004, **92**, 027003
- [17] U. Eibenstein and W. Jung, *J. Solid State Chem.*, 1997, **133**, 21-24
- [18] K. Togano, P. Badica, Y. Nakamori, S. Orimo, H. Takeya and K. Hirata, *Phys. Rev. Lett.*, 2004, **93**, 247004
- [19] H. Q. Yuan, D. F. Agterberg, N. Hayashi, P. Badica, D. Vandervelde, K. Togano, M. Sigrist and M. B. Salamon, *Phys. Rev. Lett.*, 2006, **97**, 017006
- [20] J. Bardeen, L. N. Cooper and J. R. Schrieffer, *Phys. Rev.*, 1957, **108**, 1175-1204
- [21] N. Hayashi, K. Wakabayashi, P. A. Frigeri and M. Sigrist, *Phys. Rev. B.*, 2006, **73**, 024504
- [22] P. Badica, T. Kondo and K. Togano, *J. Phys. Soc. Jpn.*, 2005, **74**, 1014-1019
- [23] E. M. Carnicom, W. Xie, T. Klimczuk, J. Lin, K. Górnicka, Z. Sobczak, N. P. Ong and R. J. Cava, *Sci. Adv.*, 2018, **4**, eaar7969
- [24] S. Foner and E. J. McNiff Jr., *Phys. Lett. A*, 1973, **45**, 429-430
- [25] Y. Watanabe, H. Arima, A. Yamashita, A. Miura, C. Moriyoshi, Y. Goto, C.-H. Lee, R. Higashinaka, H. Usui, S. Kawaguchi, K. Hoshi and Y. Mizuguchi, *J. Am. Chem. Soc.*, 2024,

146, 773-781

[26] S. Iijima, *Nature*, 1991, **354**, 56-58

[27] P. J. F. Harris, *Cambridge Univ. Press*, 2009

[28] C. Bäuml, L. Bauriedl, M. Marganska, M. Grifoni, C. Strunk and N. Paradiso, *Nano Lett.*, 2021, **21**, 8627-8633

[29] R. Tenne, L. Margulis, M. Genut and G. Hodes, *Nature*, 1992, **360**, 444-446

[30] W. Shi, J. Ye, Y. Zhang, R. Suzuki, M. Yoshida, J. Miyazaki, N. Inoue, Y. Saito and Y. Iwasa, *Sci. Rep.*, 2015, **5**, 12534

[31] H. Alpern, E. Katzir, S. Yochelis, N. Katz, Y. Paltiel and O. Millo, *New J. Phys.*, 2016, **18**, 113048

[32] H. Alpern, K. Yavilberg, T. Dvir, N. Sukenik, M. Klang, S. Yochelis, H. Cohen, E. Grosfeld, H. Steinberg, Y. Paltiel and O. Millo, *Nano Lett.*, 2019, **19**, 5167–5175

[33] H. Alpern, M. Amundsen, R. Hartmann, N. Sukenik, A. Spuri, S. Yochelis, T. Prokscha, V. Gutkin, Y. Anahory, E. Scheer, J. Linder, Z. Salman, O. Millo, Y. Paltiel and A. D. Bernardo, *Phys. Rev. Materials*, 2021, **5**, 114801

[34] Z. Wan, G. Qiu, H. Ren, Q. Qian, Y. Li, D. Xu, J. Zhou, J. Zhou, B. Zhou, L. Wang, T.-H. Yang, Z. Sofer, Y. Huang, K. L. Wang and X. Duan, *Nature*, 2024, <https://doi.org/10.1038/s41586-024-07625-4>

[35] Y. Gao, Y. Pan, J. Zhou and L. Zhang, *Phys. Rev. B*, 2023, **108**, 064510

[36] R. Mitsuhashi, Y. Suzuki, Y. Yamanari, H. Mitamura, T. Kambe, N. Ikeda, H. Okamoto, A. Fujiwara, M. Yamaji, N. Kawasaki, Y. Maniwa and Y. Kubozono, *Nature*, 2010, **464**, 76-79

[37] X. Wang, R. Liu, Z. Gui, Y. Xie, Y. Yan, J. Ying, X. Luo and X. Chen, *Nat. Commun.*, 2011, **2**, 507

[38] M. Xue, T. Cao, D. Wang, Y. Wu, H. Yang, X. Dong, J. He, F. Li and G. F. Chen, *Sci. Rep.*, 2012, **2**, 389

[39] F. Pop, N. Zigon and N. Avarvari, *Chem. Rev.*, 2019, **119**, 8435-8478

- [40] B. Yang, L. Liu, T. J. Katz, C. A. Liberko and L. L. Miller, *J. Am. Chem. Soc.*, 1991, **113**, 8993-8994
- [41] C. A. Liberko, L. L. Miller, T. J. Katz and L. Liu, *J. Am. Chem. Soc.*, 1993, **115**, 2478-2482
- [42] S. Heguri, M. Kobayashi and K. Tanigaki, *Phys. Rev. B*, 2015, **92**, 014502
- [43] F. D. Romero, M. J. Pitcher, C. I. Hiley, G. F. S. Whitehead, S. Kar, A. Y. Ganin, D. Antypov, C. Collins, M. S. Dyer, G. Klupp, R. H. Colman, K. Prassides and M. J. Rosseinsky, *Nat. Chem.*, 2017, **9**, 644-652
- [44] Y. Takabayashi, M. Menelaou, H. Tamura, N. Takemori, T. Koretsune, A. Štefančič, G. Klupp, A. J. C. Buurma, Y. Nomura, R. Arita, D. Arčon, M. J. Rosseinsky and Kosmas Prassides, *Nat. Chem.*, 2017, **9**, 635-643
- [45] T. Ishiguro, K. Yamaji and G. Saito, *Organic Superconductors*. Heidelberg, Springer-Verlag, 1998
- [46] N. Thorup, G. Rindorf, H. Soling and K. Bechgaard, *Acta Cryst. B*, 1981, **37**, 1236-1240
- [47] D. Jérôme, A. Mazaud, M. Ribault, K. Bechgaard, *J. Phys. Lett.*, 1980, **41**, L95-L98
- [48] E. B. Yagubskii, I. F. Shchegolev, V. N. Laukhin, P. A. Kononovich, M. V. Karatsovnik, A. V. Zvarykina and L. I. Buravov, *JETP Lett.*, 1984, **39**, 12-16
- [49] S. Uji, H. Shinagawa, T. Terashima, T. Yakabe, Y. Terai, M. Tokumoto, A. Kobayashi, H. Tanaka and H. Kobayashi, *Nature*, 2001, **410**, 908-910
- [50] K. Miyagawa, K. Kanoda and A. Kawamoto, *Chem. Rev.*, 2004, **104**, 5635-5654
- [51] T. Komatsu, T. Nakamura, N. Matsukawa, H. Yamochi, G. Saito, H. Ito, T. Ishiguro, M. Kusunoki, K. Sakaguchi, *Solid State Commun.*, 1991, **80**, 843-847.
- [52] H. Urayama, H. Yamochi, G. Saito, K. Nozawa, T. Sugano, M. Kinoshita, S. Sato, K. Oshima, A. Kawamoto, and J. Tanaka, *Chem. Lett.*, 1988, **17**, 55-58
- [53] S. Fujio, K. Tanaka, H. Inui, R. Ueji, N. Sumida, H. Yamochi and G. Saito, *J. Appl. Crystallogr.*, 2009, **42**, 433-441

- [54] P. A. Mansky, P. M. Chaikin and R. C. Haddon, *Phys. Rev. B*, 1994, **50**, 15929-15944
- [55] W.-Y. He and K. T. Law, *Phys. Rev. Res.*, 2020, **2**, 012073(R)
- [56] V. M. Edelstein, *Solid State Commun.*, 1990, **73**, 233-235
- [57] V. M. Edelstein, *Phys. Rev. Lett.*, 1995, **75**, 2004-2007
- [58] T. J. Blundell, M. Brannan, H. Nishimoto, T. Kadoya, J. Yamada, H. Akutsu, Y. Nakazawa and L. Martin, *Chem. Commun.*, 2021, **57**, 5406-5409
- [59] T. J. Blundell, J. R. Lopez, K. Sneade, J. D. Wallis, H. Akutsu, Y. Nakazawa, S. J. Coles, C. Wilson and L. Martin, *Dalton Trans.*, 2022, **51**, 4843-4852
- [60] N. Avarvari and J. D. Wallis, *J. Mater. Chem.*, 2009, **19**, 4061-4076
- [61] N. Mroweh, P. Auban-Senzier, N. Vanthuyne, E. Canadell and N. Avarvari, *J. Mater. Chem. C*, 2019, **7**, 12664-12673
- [62] F. Pop, P. Auban-Senzier, A. Frąckowiak, K. Ptaszyński, I. Olejniczak, J. D. Wallis, E. Canadell and Narcis Avarvari, *J. Am. Chem. Soc.*, 2013, **135**, 17176-17186
- [63] J. R. Galán-Mascarós, E. Coronado, P. A. Goddard, J. Singleton, A. I. Coldea, J. D. Wallis, S. J. Coles and Antonio Alberola, *J. Am. Chem. Soc.*, 2010, **132**, 9271-9273
- [64] F. Pop, C. Mézière, M. Allain, P. Auban-Senzier, N. Tajima, D. Hirobe, H. M. Yamamoto, E. Canadell and N. Avarvari, *J. Mater. Chem. C*, 2021, **9**, 10777-10786
- [65] F. Pop, P. Auban-Senzier, E. Canadell and N. Avarvari, *Chem. Commun.*, 2016, **52**, 12438-12441
- [66] F. Pop, P. Auban-Senzier, E. Canadell, G. L. J. A. Rikken and N. Avarvari, *Nat. Commun.*, 2014, **5**, 3757
- [67] J. S. Zambounis, C. W. Mayer, K. Hauenstein, B. Hilti, W. Hofherr, J. Pfeiffer, M. Bürkle and G. Rihs, *Adv. Mater.*, 1992, **4**, 33-35
- [68] N. Mroweh, C. Mézière, F. Pop, P. Auban-Senzier, P. Alemany, E. Canadell and N. Avarvari, *Adv. Mater.*, 2020, **32**, 2002811
- [69] H. B. Cui, H. Kobayashi, S. Ishibashi, M. Sasa, F. Iwase, R. Kato and A. Kobayashi, *J.*

Am. Chem. Soc., 2014, **136**, 7619-7622

[70] F. Pop and N. Avarvari, *Coord. Chem. Rev.*, 2017, **346**, 20-31

[71] D. G. Branzea, F. Pop, P. Auban-Senzier, R. Clérac, P. Alemany, E. Canadell and N. Avarvari, *J. Am. Chem. Soc.*, 2016, **138**, 6838-6851